Entpd5 is essential for skeletal mineralization and regulates phosphate homeostasis in zebrafish

Leonie F. A. Huitema[a], Alexander Apschner[a], Ive Logister[a], Kirsten M. Spoorendonk[a], Jeroen Bussmann[a], Chrissy L. Hammond[a,1], and Stefan Schulte-Merker[a,b,2]

[a]Hubrecht Institute, Royal Netherlands Academy of Arts and Sciences and University Medical Centre Utrecht, 3584 CT, Utrecht, The Netherlands; and [b]Experimental Zoology Group, Department of Animal Sciences, Wageningen University, 6709 PG, Wageningen, The Netherlands

Edited* by Clifford J. Tabin, Harvard Medical School, Boston, MA, and approved November 12, 2012 (received for review August 17, 2012)

Bone mineralization is an essential step during the embryonic development of vertebrates, and bone serves vital functions in human physiology. To systematically identify unique gene functions essential for osteogenesis, we performed a forward genetic screen in zebrafish and isolated a mutant, *no bone* (*nob*), that does not form any mineralized bone. Positional cloning of *nob* identified the causative gene to encode *ectonucleoside triphosphate/diphosphohydrolase 5* (*entpd5*); analysis of its expression pattern demonstrates that *entpd5* is specifically expressed in osteoblasts. An additional mutant, *dragonfish* (*dgf*), exhibits ectopic mineralization in the craniofacial and axial skeleton and encodes a loss-of-function allele of *ectonucleotide pyrophosphatase phosphodiesterase 1* (*enpp1*). Intriguingly, generation of double-mutant *nob/dgf* embryos restored skeletal mineralization in *nob* mutants, indicating that mechanistically, Entpd5 and Enpp1 act as reciprocal regulators of phosphate/pyrophosphate homeostasis in vivo. Consistent with this, *entpd5* mutant embryos can be rescued by high levels of inorganic phosphate, and phosphate-regulating factors, such as *fgf23* and *npt2a*, are significantly affected in *entpd5* mutant embryos. Our study demonstrates that Entpd5 represents a previously unappreciated essential player in phosphate homeostasis and skeletal mineralization.

The vertebrate skeleton is composed of bone and cartilage. Bone-forming cells, osteoblasts, secrete a collagen-rich matrix that is subsequently mineralized, whereas bone-resorbing cells, osteoclasts, remove bone tissue and remodel it. Osteoblasts are of mesenchymal origin, and Runx2 and Osterix have been identified as the major transcription factors controlling osteoblast commitment and differentiation (1, 2). Osteoclasts, on the other hand, are of hematopoietic origin and derive from the monocyte lineage (3). In humans, the generation and remodeling of bone is a dynamic process that occurs throughout life and is dependent on age and sex. A number of human osteopathies are common, often caused by misregulation of skeletal mineral homeostasis (mainly calcium and phosphate).

Crucial in regulating biomineralization is the balance between promoters and inhibitors of biomineralization, both on an autocrine/paracrine level as well as on a systemic level. The ratio between phosphate and pyrophosphate is central to this process. Locally, in the osteoblast and its microenvironment, phosphatases such as phosphatase orphan 1 (PHOSPHO1) or tissue-nonspecific alkaline phosphatase (TNAP) are thought to be key factors in the initiation of mineralization (4). PHOSPHO1 is responsible for providing the phosphate necessary for nucleation of crystal growth within matrix vesicles (5), whereas TNAP can dephosphorylate various substrates but most importantly breaks down pyrophosphate in the microenvironment of osteoblasts (6). Pyrophosphate is a strong chemical inhibitor of bone mineral (hydroxyapatite) formation and is locally provided by the pyrophosphate channel ANK and ectonucleotide pyrophosphatase phosphodiesterase 1 (ENPP1) (7). On a whole-organism level, phosphate levels are regulated by controlling retention/secretion in the kidney via a hormonal network involving parathyroid hormone (PTH), FGF23, and $1,25(OH)_2D_3$ (8).

Under normal conditions, calcium and phosphate concentrations of the extracellular fluid are below the level of saturation needed for spontaneous precipitation in soft tissues but above the level sufficient to support crystal growth in skeletal tissue (9). For example, deficiency in the ENPP1 gene can result in pathological soft-tissue mineralization, particularly in arteries (10, 11). On the other hand, hypophosphatemia leads to decreased mineralization of skeletal tissues, as evidenced by genetic studies in which PHOSPHO1, PHEX (phosphate regulating gene with homologies to endopeptidases on the X chromosome), or TNAP function is diminished (4, 12, 13).

We have taken a forward genetic approach to identify novel regulators of osteogenesis and bone mineralization, and here report the isolation and characterization of two zebrafish mutants: *no bone* (*nob*) mutants fail to form any mineralized skeleton, whereas *dragonfish* (*dgf*) mutants show ectopic mineralization in the craniofacial and axial skeleton. We demonstrate the causative genes to encode Entpd5 (ectonucleoside triphosphate/diphosphohydrolase 5) and Enpp1, respectively, and provide evidence that the combined activity of these factors maintains normal physiological levels of phosphate and pyrophosphate in the embryo.

Results

***Nob* Mutants Lack a Mineralized Skeleton.** In a forward genetic screen in zebrafish (14), we uncovered 14 mutant lines out of 429 families screened. One mutant, *no bone* (nob^{hu3718}), completely lacked a mineralized skeleton (Fig. 1 *A* and *B*). Skeletal staining of mutant and sibling embryos showed that the mutant phenotype is apparent at 6 d postfertilization (dpf) (Fig. 1*A*). *Nob* mutant embryos maintained the ability to form mineralized teeth and otoliths (Fig. 1*A*), two calcified structures with a different mineral composition from bone (15, 16). Mutant embryos were viable when separated at 6 dpf from their siblings via alizarin red-based in vivo skeletal staining (17). Except for the absence of a mineralized skeleton (Fig. 1*B*), we could not phenotypically distinguish mutants from siblings until 21 dpf (Fig. 1*C*). After about 21 dpf, *nob* mutants showed slower growth and died around 35 dpf.

Dermal bone formation (which does not occur via a cartilaginous intermediate) is equally affected in *nob* mutants, indicating

Author contributions: L.F.A.H., A.A., I.L., K.M.S., C.L.H., and S.S.-M. designed research; L.F.A.H., A.A., I.L., K.M.S., J.B., and C.L.H. performed research; J.B. contributed new reagents/analytic tools; L.F.A.H., A.A., I.L., K.M.S., J.B., C.L.H., and S.S.-M. analyzed data; and L.F.A.H., A.A., J.B., C.L.H., and S.S.-M. wrote the paper.

The authors declare no conflict of interest.

*This Direct Submission article had a prearranged editor.

Data deposition: The data reported in this paper have been deposited in the Gene Expression Omnibus (GEO) database, www.ncbi.nlm.nih.gov/geo (accession no. GSE35737).

[1]Present address: Departments of Biochemistry, Physiology, and Pharmacology, University of Bristol, Bristol BS8 1TD, United Kingdom.

[2]To whom correspondence should be addressed. E-mail: s.schulte@hubrecht.eu.

This article contains supporting information online at www.pnas.org/lookup/suppl/doi:10.1073/pnas.1214231110/-/DCSupplemental.

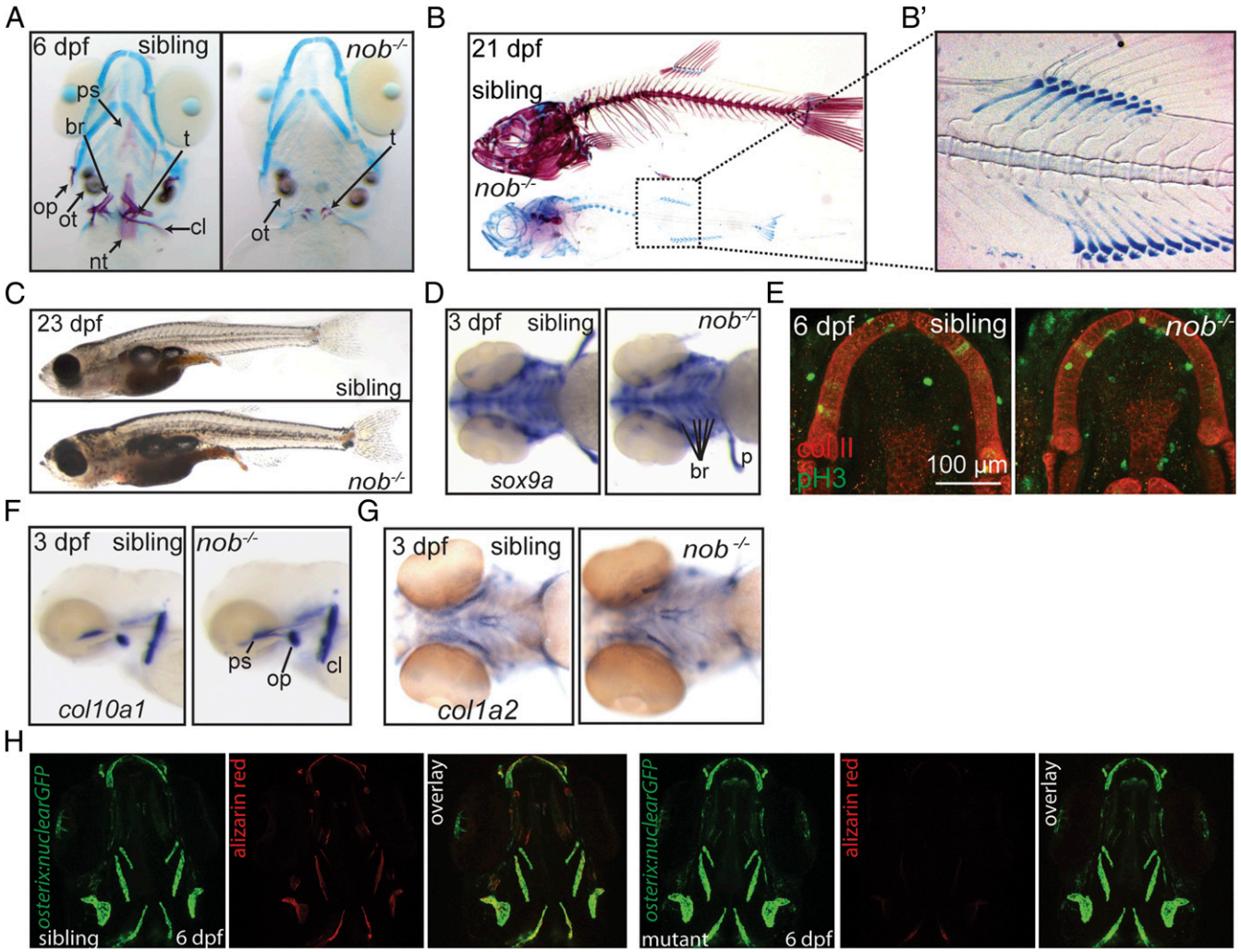

Fig. 1. *Nob* mutants lack a mineralized skeleton. (*A*) Alizarin red/alcian blue staining of sibling and mutant *nob* embryos. Cartilage elements appear normal in mutants. All bone is absent, but teeth and otoliths are present. (*B*) Skeletal staining of 21-dpf sibling and *nob* mutant individuals. (*B′*) Enhanced contrast image highlighting the correctly patterned but unmineralized vertebra anlagen. (*C*) Images of sibling and mutant *nob* fish at 23 dpf, demonstrating that *nob* mutants are indistinguishable from siblings at the gross morphological level. (*D*) Whole-mount in situ hybridization detecting the chondrogenic marker *sox9a*. (*E*) Confocal projection of Meckel's cartilage of a sibling versus mutant embryo showing no difference for anti-type II collagen (red) or the proliferation marker anti–phospho-Histone H3 (green). (*F* and *G*) Whole-mount in situ hybridization detecting the osteoblast markers *col10a1* (*F*) and *col1a2* (*G*) in 3-dpf *nob* mutant and sibling embryos. (*H*) *Osterix*:GFP expression, marking early osteoblasts in 6-dpf *nob* mutant and sibling embryos. br, fifth branchial arch; cl, cleithrum; nt, notochord tip; op, operculum; ot, otolith; ps, parasphenoid; t, teeth.

that the phenotype is not caused by chondrogenesis defects. Nevertheless, we asked whether cartilage tissue develops normally in *nob* mutants. Alcian blue staining, labeling mucopolysaccharides and glycosaminoglycans in cartilage, appeared identical in mutant versus sibling embryos (Fig. 1*A* and Fig. S1*A*). We visualized the expression of *sox9a* and type II collagen but could not find qualitative difference in the expression of these chondrogenic markers (Fig. 1 *D* and *E*). We also analyzed the proliferation marker phospho-Histone H3 (pH3) in 6-dpf *nob* mutants ($n = 4$; average of 9.00 pH3-positive chondrocytes) versus siblings ($n = 4$; average of 12.75 chondrocytes). Again, this did not constitute a significant difference in proliferating cells in the craniofacial elements (Fig. 1*E*). Together, these data suggest that chondrogenesis is unaltered in *nob* mutants.

Next, we asked whether an absence of osteoblasts might be causative for the *nob* mutant phenotype, and addressed this question using an *osterix*:GFP transgenic line (17, 18) as well as other osteoblast markers. As shown in Fig. 1 *F–H*, no difference was observed in the number of *osterix* (Fig. 1*H*)-expressing osteoblasts between sibling and *nob* mutant embryos. In addition, we observed no difference in the expression of *type I collagen* (*col1a2*) (Fig. 1*G*) or *type 10 collagen* (*col10a1*) (Fig. 1*F*), which marks osteoblasts in teleosts (19). Together, these data demonstrate that it is not the absence of osteoblasts that is causative for the *nob* mutant phenotype.

***Nob* Mutants Encode Alleles of *entpd5*.** To identify the molecular lesion responsible for the nob^{hu3718} mutant phenotype, we used simple sequence-length polymorphism and single-nucleotide polymorphism mapping. Single-embryo mapping positioned the mutation between flanking markers SNP-Z8 and CA39 (Fig. 2*A*) on chromosome 17. Sequencing of the zebrafish *entpd5* gene (in mammals also referred to as CD39L4 or PCPH) in mutant and sibling embryos using gene specific primers (Table S1) revealed a premature stop codon in the mutant allele due to a T→A transversion in the third coding exon (Fig. 2*B*). This mutation resulted in a Leu>stop alteration at position 155, which is in the second apyrase conserved domain (gray bars in Fig. 2*D*, *Upper*)

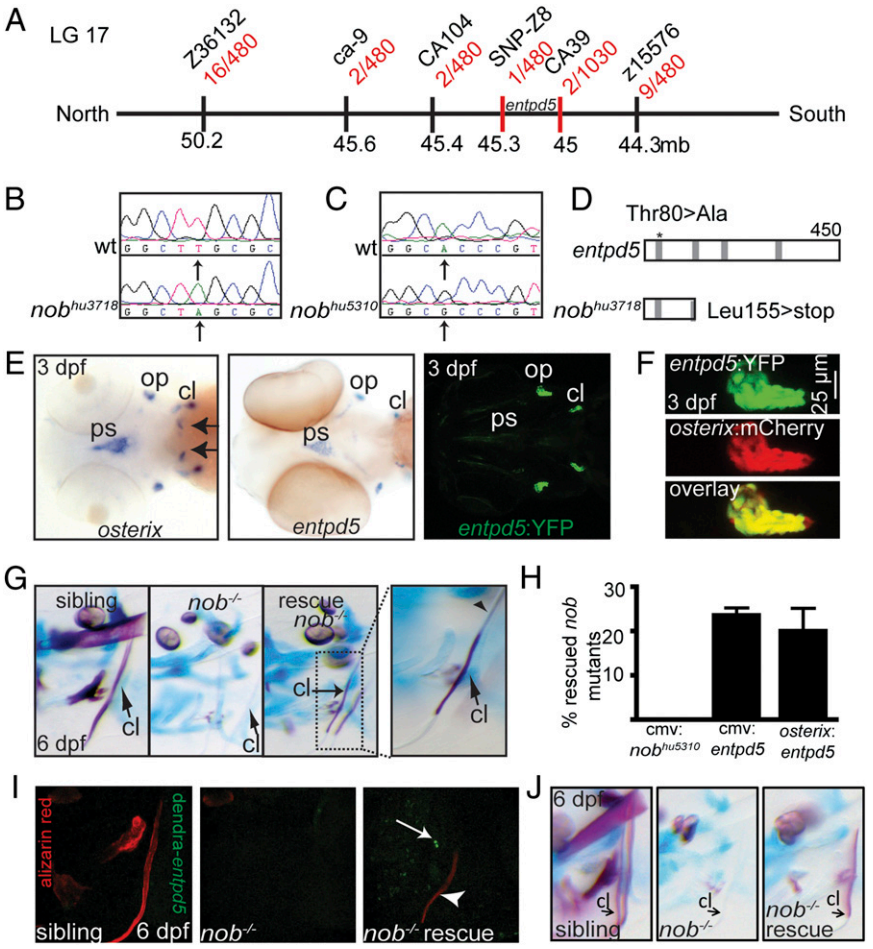

Fig. 2. *Nob* mutants encode *entpd5*, which is specifically expressed in osteoblasts. (*A*) Meiotic map of the nob^{hu3718} locus. Recombinants per total number of mutants tested for each polymorphic marker are depicted in red, and markers used for mapping are in black. (*B*) Sequencing of nob^{hu3718} revealed a Leu155>stop mutation. (*C*) Sequencing of nob^{hu5310} revealed a Thr80>Ala mutation transversion. (*D*) Schematic representation of the predicted protein structures for Entpd5 and nob^{hu3718}. The asterisk indicates the position of the mutation in nob^{hu5310}. Gray bars, apyrase domains within Entpd5 (35). See also Fig. S1. (*E*) (*Left* and *Center*) *Entpd5* and *osterix* are almost identically expressed in 3-dpf embryos, with *osterix* expression in the region of future teeth (arrows) being the single exception at this stage. (*Right*) Representative image of a 3-dpf *entpd5*:YFP transgenic embryo showing an expression pattern that matches endogenous *entpd5* transcript distribution (*Center*). (*F*) Coexpression of *entpd5*:YFP and *osterix*:mCherry in the operculum of 3-dpf embryos. (*G* and *H*) *entpd5* cDNA injection (CMV promoter) into nob^{hu3718} mutants results in mosaic mineralization (*G*). Arrows point at cleithra in *G*; the arrowhead points to a nonmineralized osteoid in a partially mineralized cleithrum. Bar graphs in *H* represent percentages of rescued mutant embryos at 6 dpf (expressed as mean ± SEM, three independent experiments). (*I*) Alizarin red staining of a mutant *nob* embryo that had been injected with a cmv:dendra-t2a-*entpd5* expression construct at the one-cell stage. The cleithrum is partially mineralized in the mutant (arrowhead); however, there are no dendra-positive cells immediately abutting the mineralized structure (arrow). (*J*) Representative example of an embryo partially rescued by endothelial-specific expression of *entpd5* (*kdr-like*:*entpd5*).

of the predicted protein. We also uncovered a separate, noncomplementing allele (nob^{hu5310}). The nob^{hu5310} allele contained an A→G transversion in the first coding exon (Fig. 2*C*), resulting in a Thr>Ala alteration at position 80 (asterisk in Fig. 2*D*). This mutation is located in a highly conserved amino acid residue of the first apyrase conserved domain (see also Fig. S1*B*).

***Entpd5* Expression Is Sufficient to Rescue the *nob* Phenotype.** Next, we studied the expression pattern of *entpd5* by whole-mount in situ hybridization. *Entpd5* and *osterix* showed an almost identical expression pattern at 3 dpf, with *osterix* expression in the region of future teeth as the single exception at this stage (Fig. 2*E*). To confirm that *osterix*-positive cells also express *entpd5*, we generated an *entpd5*:YFP transgenic line. As shown in Fig. 2*E* (*Center* and *Right*), YFP expression was identical to the endogenous *entpd5* gene expression. We crossed the *entpd5*:YFP transgenic line with the *osterix*:mCherry transgenic line and observed that *osterix*-expressing cells also express *entpd5* (Fig. 2*F*), demonstrating that *entpd5* is specifically expressed in, and can serve as a marker for, osteoblasts. Of note, at all stages analyzed, we only observed *entpd5* expression in tissues associated with skeletal mineralization.

To provide independent evidence that the mutations in the two mutant *entpd5* alleles are causative for the *nob* phenotype, we attempted to rescue the phenotype by injection of wild-type and nob^{hu5310} mutant *entpd5* cDNA under the control of a cytomegalovirus (CMV) promoter. Mosaic rescue (as expected upon plasmid DNA injection) was observed in 24% of the nob^{hu3718} mutants that were injected with wild-type cDNA (Fig. 2 *G* and *H*), whereas the mutant nob^{hu5310} *entpd5* cDNA failed to rescue. Of note, rescued embryos showed only mineralization in skeletal elements, not in other parts of the embryo. Mineralization was similarly rescued when wild-type *entpd5* cDNA was expressed in the rescuing assay under the control of the *osterix* promoter (Fig. 2*H*).

Next, we visualized the (mosaic) location of *entpd5*-positive cells of rescued *nob* mutants, and therefore injected a cmv:dendra-t2a-*entpd5* construct to mark the cells in which the *entpd5* gene was overexpressed. Surprisingly, we observed that mineralization was rescued even if osteoblasts do not inherit detectable levels of cmv:dendra-t2a-*entpd5* (Fig. 2*I*). This prompted us to force *entpd5* expression in a tissue distinct from osteoblasts, to clarify the question of whether Entpd5 function needs to be provided by osteoblasts or can be provided by other tissues. Interestingly, injections of *entpd5* under the control of an endothelial-specific promoter (*kdrl*:*entpd5*) (20) resulted in rescue of *nob* mutants in a manner indistinguishable from the cases described above (Fig. 2*J*). These results show that although Entpd5 is essential for mineralization and is expressed by osteoblasts in the wild-type embryo, it can be provided by other cellular sources and does not need to be delivered by osteoblasts.

***Dragonfish* Mutants Encode Alleles of *enpp1*.** In the same genetic screen we also uncovered a mutant, termed *dragonfish* (*dgf*), that displayed an ectopic mineralization phenotype (Fig. 3 *A* and *B*) in the axial skeleton with apparent fusion of the mineralized vertebral centra (Fig. 3*A*) and also displayed bone nodules at characteristic positions of the cleithrum (arrow in Fig. 3*B*). Single-embryo mapping positioned the mutation between two flanking markers, SSLR 210 and SSLR 961 (Fig. 3*C*), on chromosome 20.

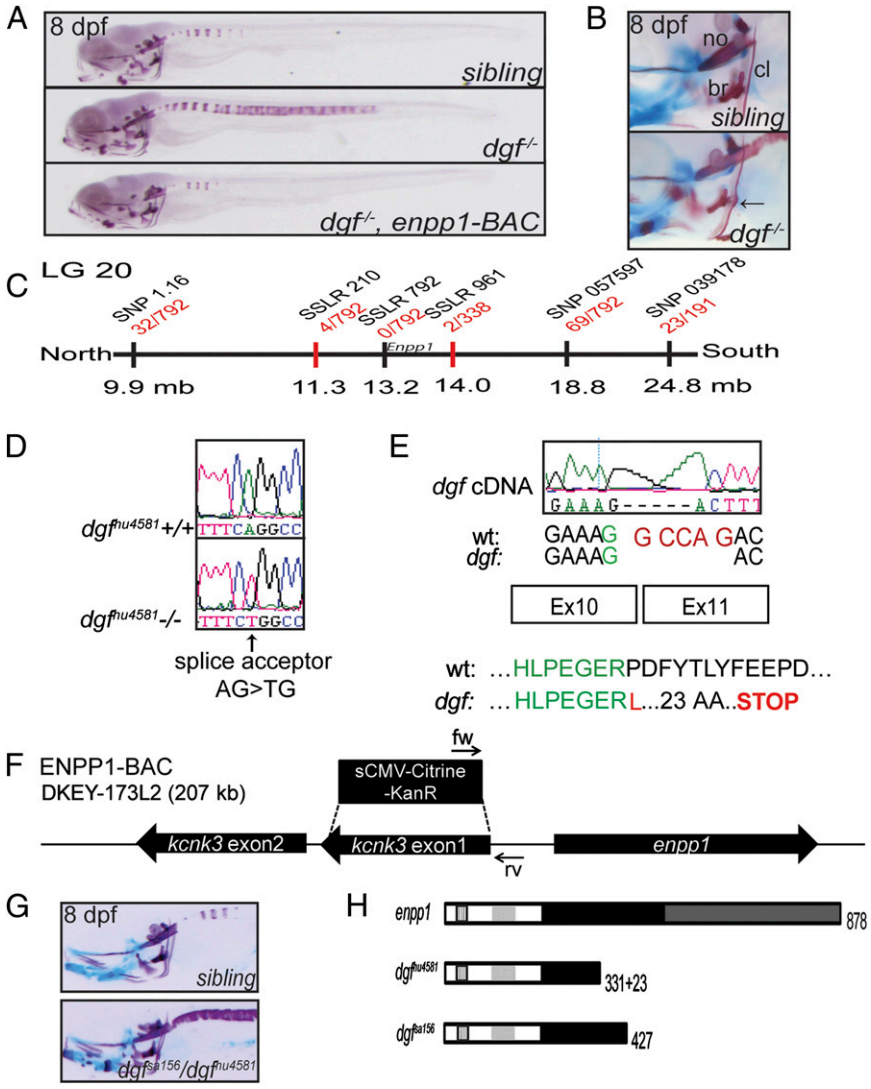

Fig. 3. Ectopic mineralization phenotypes in *dgf* mutants. (*A*) Skeletal staining of a sibling, a *dgf* mutant, and a *dgf* mutant rescued by an *enpp1* BAC transgene. *Dgf* mutants exhibit axial hypermineralization, resulting in partially fused vertebral centra. (*B*) Hypermineralization also affects the cleithra, which in *dgf* mutants typically exhibit nodule-like protrusions (arrow). no, notochord. (*C*) Meiotic map of the *dgf* locus. Recombinants per total number of mutants tested for each polymorphic marker are depicted in red, and markers used for mapping are in black. (*D*) Sequencing of dgf^{hu4581} revealed a mutation in the splice acceptor site before exon 11 of the *enpp1* gene. (*E*) The consequence at the transcript level is a deletion of 5 bp (*Upper*), resulting in a translational frameshift and a predicted stop codon after 23 amino acids (*Lower*). (*F*) Schematic representation of the BAC construct generated for the transgenic rescue of the dgf^{4581} phenotype. Two genes are contained on the BAC, and *kcnk3* was inactivated through a recombineering approach. (*G*) Dgf^{sa156} fails to complement dgf^{hu4581}. (*H*) Schematic drawing of the predicted protein forms of *enpp1*, dgf^{hu4581}, and dgf^{sa156}, respectively. Enpp1 is a type II transmembrane protein. Striped box, transmembrane domain; light gray, somatomedin B-like binding domains; black, catalytic domain; dark gray, nuclease-like domain (36). See also Fig. S2.

Sequencing (Fig. 3 *D* and *E*) of two noncomplementing alleles (Fig. 3 *G* and *H* and Fig. S2*C*) as well as a BAC-mediated rescue (Fig. 3 *A* and *F* and Fig. S2 *A* and *B*) identified mutations within the *enpp1* gene underlying the mutant phenotype.

Phosphate Homeostasis Is Disturbed in *nob* Mutants. Entpd5 and Enpp1 both hydrolyze extracellular nucleotide derivatives (7, 10, 11, 21, 22), with Entpd5 generating inorganic phosphate (21, 22) and Enpp1 generating pyrophosphate (7). We therefore examined the epistatic relationship of both genes. Strikingly, double-mutant *nob*/*dgf* embryos always formed mineralized bone and usually even exhibited signs of an ectopically mineralized skeleton (Fig. 4*A*). As this suggested that phosphate homeostasis is disturbed in *nob* mutants, we tested whether raising *nob* mutant embryos in excess phosphate medium would be sufficient to rescue the phenotype. Indeed, growing embryos in phosphate-rich medium resulted in partial skeletal mineralization of *nob* mutants (Fig. 4*B*), demonstrating that inorganic phosphate is a limiting factor for *nob* mutants to mineralize their skeleton. Of note, excess calcium had no effect on the *nob* phenotype, whereas exogenously supplied calcium has been shown to rescue other mutants with hypomineralized phenotypes (23, 24).

Next, we studied whether phosphate-regulating genes were affected in *nob* mutants. Two independent microarray experiments on 7-dpf *nob* sibling versus mutant embryos (see *SI Materials and Methods*) demonstrated strong down-regulation of the key phosphate homeostasis regulator fibroblast growth factor 23 (*fgf23*) in *nob* mutants. Significant twofold down-regulation of *fgf23* was validated by quantitative (q)PCR (Fig. 4*C*), but this difference could be ameliorated by supplying Entpd5 via injection of *kdrl:entpd5* (Fig. S3). In addition to this, we studied the expression of several other phosphate-regulating genes (which were not present on the array chip; Fig. S1) by qPCR (Fig. 4*C*). In concordance with *fgf23* down-regulation, significant up-regulation of the sodium/phosphate cotransporter *npt2a* was measured in 7-dpf *nob* mutants (Fig. 4*C*).

Taken together, our findings show that Entpd5 is an essential factor for bone mineralization, and indicate that, mechanistically, Entpd5 acts on phosphate/pyrophosphate homeostasis.

Discussion

We here show that Entpd5 is crucial for bone mineralization in zebrafish and that *entpd5* is specifically expressed in osteoblasts. Taken together, our findings show that Entpd5 is a previously unappreciated and essential factor for bone formation. Entpd5 encodes a secreted ectonucleoside triphosphate/diphosphohydrolase that preferably hydrolyzes extracellular nucleotide diphosphates (21, 22) into nucleotide monophosphates and inorganic phosphate. Circulating extracellular nucleotides are known to be important purinergic signaling molecules that can

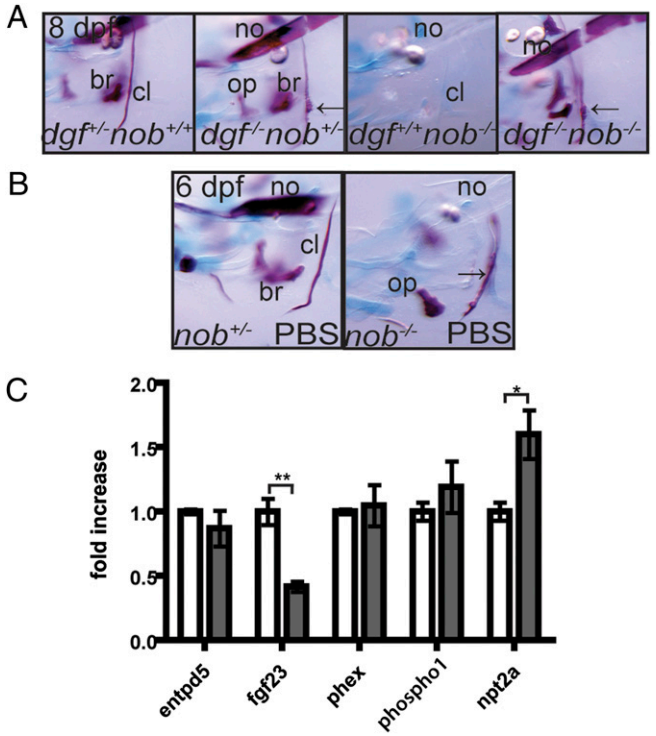

Fig. 4. Phosphate homeostasis is disturbed in *nob* mutants. (*A*) *Nob* mutants can mineralize their skeleton in the absence of dgf^{hu4581} function, and will even show ectopic mineralization (arrows point at protrusions of the cleithrum, a typical feature of *dgf* mutants). (*B*) Exogenous phosphate partially rescues the *nob* mutant phenotype. Arrow points at partially mineralized cleithrum. All images represent lateral views of the head skeleton at 6 dpf. (*C*) Quantitative PCR on 7-dpf embryos revealed that, compared with siblings (white bars), *fgf23* expression levels are significantly down-regulated and *npt2a* expression is significantly up-regulated in *nob* mutant embryos (gray bars). Results are expressed as mean ± SEM of three independent experiments, with $*P < 0.05$ and $**P < 0.005$.

generate a variety of physiological responses (25, 26). Although we do not exclude the possibility of an additional role of purinergic signaling in skeletal mineralization (26), our data rather point to a role of Entpd5 in phosphate homeostasis.

The restricted expression pattern of *entpd5* in osteoblasts suggests that Entpd5 acts locally, in a microenvironment that is already permissive for mineralization. On one hand, this notion is supported by the rescue experiments reported here: Expression of *entpd5* via a ubiquitously acting CMV promoter or an endothelial-specific *kdr-like* promoter does not lead to ectopic mineralization, but results exclusively in bone mineralization in those regions where the local microenvironment (extracellular matrix composition, pyrophosphate levels) is prone to mineralization events. On the other hand, *entpd5* does not need to be provided in a cell-autonomous manner (i.e., in osteoblasts): Expression in the embryonic endothelium is sufficient to cause mineralization. In the wild-type embryo, one would still expect the highest levels of Entpd5 protein at the osteoblast surface, and therefore in the immediate vicinity of a microenvironment that provides the appropriate and required composition for biomineralization (see Fig. S4 for a model).

Entpd5 has recently been suggested to play a role in proper protein folding and glycosylation in the endoplasmic reticulum (27). However, because both the cartilage matrix and the osteoid appeared normal in *nob* mutants, and because *dgf*/*nob* double mutants can mineralize their skeleton, we consider it unlikely that a failure of proper glycosylation of extracellular matrix proteins is the limiting factor for skeletal mineralization. Rather, our data strongly suggest that a stringently controlled balance between Entpd5 and Enpp1 activities determines the level of mineralization through controlling the ratio of inorganic phosphate to pyrophosphate in the immediate vicinity of osteoblasts. Skeletal mineralization is a tightly controlled process, depending on the availability of inorganic phosphate release from a variety of substrates by ectoenzymes (7). Pyrophosphate antagonizes the ability of inorganic phosphate and calcium to form a mineral crystal. In line with this, *Enpp1* mutations in humans and mice have been shown to cause ectopic mineralization due to insufficient extracellular pyrophosphate (10, 11). Based on the ectopic mineralization phenotype of the *dgf* mutants, we show here on the phenotypic level that the function of Enpp1 is conserved between fish and mammals.

Because our study indicates that Entpd5 regulates phosphate homeostasis, we speculated that other factors regulating phosphate levels in vivo might be affected. Indeed, *Fgf23* is significantly down-regulated, and the sodium/phosphate cotransporter *npt2a* (NaPi2a) is significantly up-regulated in *nob* mutants. Fgf23 is known as a key regulator of phosphate homeostasis (28), and changes in FGF23 activity lead to human disorders associated with either phosphate wasting or retention (29). Fgf23 is a circulating hormone produced in the bone that mainly targets the kidneys to control the activity of Npt2a and Npt2c (30). It seems likely that the absence of skeletal mineralization in mutant *nob* zebrafish elicits compensatory mechanisms to regulate the low levels of inorganic phosphate. Down-regulation of *fgf23* and up-regulation of *npt2a* are consistent with this.

A murine Entpd5 knockout has been reported, but it is unclear whether this allele (encoding an ENTPD5:lacZ fusion) represents a complete loss-of-function situation. These mice are viable (31) but appear smaller than littermates, a phenotype often found in hypophosphatemic mice (4, 28). Furthermore, the mice were shown to have increased serum alkaline phosphatase (31). Together with the findings of our study, we believe that the phenotype reported by Read et al. (31) is likely due to disturbed phosphate homeostasis. However, we cannot exclude that the essential function of Entpd5 during osteogenesis as described here is potentially unique in basal vertebrates, and that it has shifted to other secreted paralogues in higher vertebrates, or even to completely different genes (such as alkaline phosphatase).

In summary, in this study, we demonstrate that *entpd5* is essential for skeletal mineralization in zebrafish and that *entpd5* is specifically expressed in osteoblasts. We provide evidence that the combined activity of Entpd5 and Enpp1 maintains normal physiological levels of phosphate and pyrophosphate, and that the absence of activity of either protein results in mineralization phenotypes. The *nob* mutant phenotype can be rescued by either exogenous phosphate or Entpd5 protein provided by non-osteoblast cells, suggesting that the correct systemic phosphate levels together with the appropriate extracellular microenvironment of osteogenic cells provides the basis for biomineralization.

Materials and Methods

Alizarin Red/Alcian Blue Skeletal Staining. Skeletal staining was performed as described previously (17, 32). In vivo skeletal staining was performed with 0.001% calcein or 0.05% alizarin red in E3 medium for 5–10 min and subsequent extensive washes with E3 medium.

Meiotic Mapping and Sequencing. Bioinformatic construction of the genomic region surrounding the nob^{hu3718} and dgf^{hu4581}genes was performed using Ensembl database Zv6 (http://genome.ucsc.edu/cgi-bin/hgGateway?hgsid=312908511&clade=vertebrate&org=Zebrafish&db=danRer6) for nob^{hu3718} and Zv9 (www.ensembl.org/Danio_rerio/Info/Index?db=core) for dgf^{hu4581}. Meiotic mapping of the nob^{hu3718} and dgf^{hu4581} mutations was performed using standard simple sequence-length polymorphisms and single-nucleotide polymorphisms.

For sequencing of candidate genes, coding exons of the respective gene were amplified separately from mutant and wild-type embryos and sequenced on both strands. Additional information and all primer sequences are shown in Table S1. For all experiments, we have used the *nob*^{hu3718} and *dgf*^{hu4581} alleles, unless stated otherwise.

Whole-Mount in Situ Hybridization and Immunohistochemistry. All in situ hybridizations were performed at least twice as previously described (17, 33) and embryos were subsequently genotyped. Previously described probes were *osterix* and *col10a1* (17). Immunohistochemistry was essentially done as described (18) and as detailed in *SI Materials and Methods*.

cDNA Rescue Experiments. TRIzol reagent (Invitrogen) was used to extract RNA from 6-dpf embryos, and mouse RNA was extracted from cultured KS483 cells (34). For details, please consult *SI Materials and Methods*. One-cell–stage embryos derived from *nob*^{hu3718} carrier fish were injected with plasmid DNA in a maximum volume of 2 nL. Alizarin red/alcian blue staining was carried out at 6 dpf. Only injected embryos with normal size, apparently normal cartilage, and without tissue malformations or general edema or apparent toxic defects were included for analysis. Each rescue experiment was performed three independent times. In total, we scored 490 siblings/131 mutant embryos injected with 100 pg *cmv*:*entpd5*; 329 siblings/106 mutants injected with 100 pg *osterix*:*entpd5*; 500 siblings/166 mutants with 100 pg cmv:Entpd5 (murine cDNA); 151 siblings/63 mutants with 100 pg *cmv*:*nob*^{hu5310}; and 481 sibling/129 mutants with 25 pg kdr-l:entpd5 cDNA.

Animal Procedures. All zebrafish strains were maintained at the Hubrecht Institute using standard husbandry conditions. Animal experiments were approved by the Animal Experimentation Committee of the Royal Netherlands Academy of Arts and Sciences.

ACKNOWLEDGMENTS. Members of the S,S.-M. laboratory, past and present, are acknowledged, particularly E. Mackay, G. Talsma, J. Peterson-Maduro, J. Vanoevelen, and B. Ponsioen. We thank The Sanger Centre for the *dgf*^{sa156} allele and the Hubrecht Imaging Center for expert help. S.S.-M. acknowledges support from the Smart Mix Programme of the Netherlands Ministry of Economic Affairs, the European Space Agency, TreatOA (Translational Research in Europe Applied Technologies for OsteoArthritis, FP7), and Netherlands Organization for Scientific Research (ALW2PJ/11107). A.A. is a recipient of a DOC Fellowship (Austrian Academy of Sciences).

1. Hartmann C (2009) Transcriptional networks controlling skeletal development. *Curr Opin Genet Dev* 19(5):437–443.
2. Karsenty G (2008) Transcriptional control of skeletogenesis. *Annu Rev Genomics Hum Genet* 9:183–196.
3. Teitelbaum SL (2000) Bone resorption by osteoclasts. *Science* 289(5484):1504–1508.
4. Yadav MC, et al. (2011) Loss of skeletal mineralization by the simultaneous ablation of PHOSPHO1 and alkaline phosphatase function: A unified model of the mechanisms of initiation of skeletal calcification. *J Bone Miner Res* 26(2):286–297.
5. Stewart AJ, et al. (2006) The presence of PHOSPHO1 in matrix vesicles and its developmental expression prior to skeletal mineralization. *Bone* 39(5):1000–1007.
6. Murshed M, Harmey D, Millán JL, McKee MD, Karsenty G (2005) Unique coexpression in osteoblasts of broadly expressed genes accounts for the spatial restriction of ECM mineralization to bone. *Genes Dev* 19(9):1093–1104.
7. Terkeltaub R (2006) Physiologic and pathologic functions of the NPP nucleotide pyrophosphatase/phosphodiesterase family focusing on NPP1 in calcification. *Purinergic Signal* 2(2):371–377.
8. Razzaque MS (2011) Osteo-renal regulation of systemic phosphate metabolism. *IUBMB Life* 63(4):240–247.
9. Huitema LF, Vaandrager AB (2007) What triggers cell-mediated mineralization? *Front Biosci* 12:2631–2645.
10. Okawa A, et al. (1998) Mutation in Npps in a mouse model of ossification of the posterior longitudinal ligament of the spine. *Nat Genet* 19(3):271–273.
11. Rutsch F, et al. (2003) Mutations in ENPP1 are associated with 'idiopathic' infantile arterial calcification. *Nat Genet* 34(4):379–381.
12. Tenenhouse HS (1999) X-linked hypophosphataemia: A homologous disorder in humans and mice. *Nephrol Dial Transplant* 14(2):333–341.
13. Narisawa S, Frohlander N, Millan JL (1997) Inactivation of two mouse alkaline phosphatase genes and establishment of a model of infantile hypophosphatasia. *Dev Dyn* 208(3):432–446.
14. Spoorendonk KM, Hammond CL, Huitema LFA, Vanoevelen J, Schulte-Merker S (2010) Zebrafish as a unique model system in bone research: The power of genetics and in vivo imaging. *J Appl Ichthyol* 26(2):219–224.
15. Kawasaki K, Suzuki T, Weiss KM (2005) Phenogenetic drift in evolution: The changing genetic basis of vertebrate teeth. *Proc Natl Acad Sci USA* 102(50):18063–18068.
16. Wu D, Freund JB, Fraser SE, Vermot J (2011) Mechanistic basis of otolith formation during teleost inner ear development. *Dev Cell* 20(2):271–278.
17. Spoorendonk KM, et al. (2008) Retinoic acid and Cyp26b1 are critical regulators of osteogenesis in the axial skeleton. *Development* 135(22):3765–3774.
18. Hammond CL, Schulte-Merker S (2009) Two populations of endochondral osteoblasts with differential sensitivity to Hedgehog signalling. *Development* 136(23):3991–4000.
19. Avaron F, Hoffman L, Guay D, Akimenko MA (2006) Characterization of two new zebrafish members of the hedgehog family: Atypical expression of a zebrafish indian hedgehog gene in skeletal elements of both endochondral and dermal origins. *Dev Dyn* 235(2):478–489.
20. Jin SW, Beis D, Mitchell T, Chen JN, Stainier DY (2005) Cellular and molecular analyses of vascular tube and lumen formation in zebrafish. *Development* 132(23):5199–5209.
21. Mulero JJ, Yeung G, Nelken ST, Ford JE (1999) CD39-L4 is a secreted human apyrase, specific for the hydrolysis of nucleoside diphosphates. *J Biol Chem* 274(29):20064–20067.
22. Murphy-Piedmonte DM, Crawford PA, Kirley TL (2005) Bacterial expression, folding, purification and characterization of soluble NTPDase5 (CD39L4) ecto-nucleotidase. *Biochim Biophys Acta* 1747(2):251–259.
23. Huitema LF, et al. (2012) Macrophage-stimulating protein and calcium homeostasis in zebrafish. *FASEB J* 26(10):4092–4101.
24. Vanoevelen J, et al. (2011) Trpv5/6 is vital for epithelial calcium uptake and bone formation. *FASEB J* 25(9):3197–3207.
25. Massé K, Dale N (2012) Purines as potential morphogens during embryonic development. *Purinergic Signal* 8(3):503–521.
26. Gartland A, et al. (2012) Purinergic signalling in osteoblasts. *Front Biosci* 17:16–29.
27. Fang M, et al. (2010) The ER UDPase ENTPD5 promotes protein N-glycosylation, the Warburg effect, and proliferation in the PTEN pathway. *Cell* 143(5):711–724.
28. Sitara D, et al. (2008) Genetic evidence of serum phosphate-independent functions of FGF-23 on bone. *PLoS Genet* 4(8):e1000154.
29. Lu Y, Feng JQ (2011) FGF23 in skeletal modeling and remodeling. *Curr Osteoporos Rep* 9(2):103–108.
30. Hori M, Shimizu Y, Fukumoto S (2011) Minireview: Fibroblast growth factor 23 in phosphate homeostasis and bone metabolism. *Endocrinology* 152(1):4–10.
31. Read R, et al. (2009) Ectonucleoside triphosphate diphosphohydrolase type 5 (Entpd5)-deficient mice develop progressive hepatopathy, hepatocellular tumors, and spermatogenic arrest. *Vet Pathol* 46(3):491–504.
32. Walker MB, Kimmel CB (2007) A two-color acid-free cartilage and bone stain for zebrafish larvae. *Biotech Histochem* 82(1):23–28.
33. Schulte-Merker S (2002) Looking at embryos. *Zebrafish: A Practical Approach*, eds Nüsslein-Volhard C, Dahm R (Oxford Univ Press, New York), pp 41–43.
34. Yamashita T, et al. (1996) Subcloning of three osteoblastic cell lines with distinct differentiation phenotypes from the mouse osteoblastic cell line KS-4. *Bone* 19(5):429–436.
35. Chadwick BP, Frischauf AM (1998) The CD39-like gene family: Identification of three new human members (CD39L2, CD39L3, and CD39L4), their murine homologues, and a member of the gene family from *Drosophila melanogaster*. *Genomics* 50(3):357–367.
36. Stefan C, Jansen S, Bollen M (2005) NPP-type ectophosphodiesterases: Unity in diversity. *Trends in biochemical sciences* 30(10):542–550.